Human Molecular Genetics, 2008, Vol. 17, No. 22 ***3509–3520***
doi:10.1093/hmg/ddn243
Advance Access published on August 14, 2008

The cell adhesion molecule nectin-1 is critical for normal enamel formation in mice

Martin J. Barron[1,2], Steven J. Brookes[3], Clare E. Draper[1], David Garrod[1], Jennifer Kirkham[3], Roger C. Shore[3] and Michael J. Dixon[1,2,*]

[1]Faculty of Life Sciences and [2]Dental School, University of Manchester, Michael Smith Building, Oxford Road, Manchester M13 9PT, UK and [3]Department of Oral Biology, Leeds Dental Institute, University of Leeds, Clarendon Way, Leeds LS2 9LU, UK

Received July 6, 2008; Revised and Accepted August 12, 2008

Nectin-1 is a member of a sub-family of immunoglobulin-like adhesion molecules and a component of adherens junctions. In the current study, we have shown that mice lacking nectin-1 exhibit defective enamel formation in their incisor teeth. Although the incisors of nectin-1-null mice were hypomineralized, the protein composition of the enamel matrix was unaltered. While strong immunostaining for nectin-1 was observed at the interface between the maturation-stage ameloblasts and the underlying cells of the stratum intermedium (SI), its absence in nectin-1-null mice correlated with separation of the cell layers at this interface. Numerous, large desmosomes were present at this interface in wild-type mice; however, where adhesion persisted in the mutant mice, the desmosomes were smaller and less numerous. Nectins have been shown to regulate tight junction formation; however, this is the first report showing that they may also participate in the regulation of desmosome assembly. Importantly, our results show that integrity of the SI–ameloblast interface is essential for normal enamel mineralization.

INTRODUCTION

The nectins are a sub-family of immunoglobulin-like adhesion molecules that participate in Ca^{2+}-independent cell–cell adhesion (1,2). The group comprises four members, nectins 1, 2, 3 and 4, each consisting of an extracellular region with three immunoglobulin-like loops, a single transmembrane domain and a cytoplasmic domain. Nectin-mediated adhesion is initiated by homo-*cis*-dimers, which is followed by the formation of homo-*trans*-dimers through their immunoglobulin domains (3). Hetero-*trans*-dimers form between nectin-1 and nectin-3 or -4, and between nectin-3 and -2, yielding stronger binding than homophilic interactions (3). Nectins bind to the actin cytoskeleton through the adaptor protein afadin, the PDZ domain of which binds to a conserved amino acid motif (Glu/Ala-X-Tyr-Val) at the C-terminus that is present in all except nectin-4 and the truncated splice variants of nectins-1 and -3 (4,5). Nectins are also key components of adherens junctions and are instrumental in their formation (reviewed in 2).

The nectin/afadin cell adhesion system is important for epithelial morphogenesis and organogenesis. Afadin knockout mice show embryonic lethality as the result of ectodermal defects at or following gastrulation (6). Nectin knockout mice show less severe defects presumably because of compensation between the different isoforms. Thus, mice deficient in nectin-2 or -3 have defects in sperm production and male-specific infertility (7,8) while loss of function of either nectin-1 or -3 causes microphthalmia accompanied by failure of apical contact between the pigmented and non-pigmented cells of the ciliary epithelium (9). Both nectin-1 and -3-null mice also show abnormal trajectories of mossy fibres in the hippocampus and other neural defects (10,11). In contrast, mutations of *PVRL1*, which encodes nectin-1, result in the autosomal recessive cleft lip and palate-ectodermal dysplasia syndromes Zlotogora-Ogur Syndrome

*To whom correspondence should be addressed. Tel: +44 161 275 5620; Fax: +44 161 275 5082; Email: mike.dixon@manchester.ac.uk

and Margarita Island Ectodermal Dysplasia, which are characterized by cleft lip/palate and hidrotic ectodermal dysplasia in man (12,13).

Dental enamel is unique among mammalian mineralized tissues as it is of ectodermal origin. The enamel-forming cells (ameloblasts) undergo a stereotypical series of differentiation and migration events that can be seen simultaneously in adult rodent incisor teeth, which grow and erupt continuously throughout life. An epithelial sheet, which forms apically, differentiates longitudinally towards the incisal tip into tall ameloblasts that secrete the enamel extracellular matrix and transport calcium ions to begin biomineralization (14,15). Following the secretory stage, the ameloblasts decrease in height and increase in width as they progress through the transitional stage of amelogenesis where enzyme-mediated matrix degradation occurs. Further, towards the incisal tip, the epithelium enters the maturation phase where the ameloblasts shorten further and lose secretory characteristics (14,15). Here, the removal of the matrix is completed and secondary enamel crystal growth occludes the spaces previously occupied by matrix proteins. Following maturation, the ameloblasts become cuboidal and progress forwards until they reach the gingival margin where the tooth erupts from the mandible (14,15).

Alterations in the underlying stratum intermedium (SI) accompany the morphological changes of the ameloblasts. In the secretory zone, the ameloblasts contact an SI composed of a single layer of cuboidal cells (14,15). As the ameloblasts progress to maturation, the migrating SI cells increase in size and adopt a stellate appearance. At this stage, the cells underlying the SI also increase in size and number to form the highly vascular papillary layer, which eventually decreases in size substantially at the post-maturation stage (14,15).

In the current study, we have generated mice with a null mutation of *Pvrl1*. In addition to the microphthalmia reported by Inagaki *et al*. (9), we demonstrate that *Pvrl1*$^{-/-}$ mice exhibit defective amelogenesis of their incisor teeth, which lack the normal iron pigmentation characteristic of rodent enamel and are prone to wear and breakage. This defect appears to result from loss of adhesive contact between mature ameloblasts and the underlying SI.

RESULTS

Generation of *Pvrl1*$^{-/-}$ mice

To investigate the function of nectin-1, we disrupted *Pvrl1* in mouse embryonic stem cells by homologous recombination using a gene targeting construct in which exon 1, which contains the translation initiation codon, was replaced with a neomycin-resistance cassette (Fig. 1A). Three correctly targeted embryonic stem cell lines, as assessed by Southern blot analysis (data not shown), were used to generate chimeric male mice which were inter-crossed with C57BL/6 females to generate phenotypically normal *Pvrl1*$^{\pm}$ mice, the genotypes of which were confirmed by PCR analysis (Fig. 1B). Subsequently, *Pvrl1*$^{\pm}$ mice were inter-crossed to produce homozygous mutant animals. No nectin-1 protein was detected by western blot analysis in tissues extracted from mice homozygous for the targeted locus (Fig. 1C) while heterozygotes showed an intermediate level of protein (Fig. 1C). *Pvrl1*$^{-/-}$ mice were viable and fertile but manifested microphthalmia identical to that observed in the nectin-1-null mice reported by Inagaki *et al*. (9) (data not shown).

Pvrl1$^{-/-}$ mice have abnormal incisor teeth

The enamel of both upper and lower incisor teeth of 2-month-old wild-type animals was characteristically yellow as a consequence of the deposition of iron salts (16,17) (Fig. 2A). Nectin-1-null littermates possessed a complete dentition but their upper and lower incisor teeth appeared chalky white, lacking the yellow iron pigmentation (Fig. 2B). These teeth were sometimes shorter than normal, apparently as the result of excess mechanical attrition and/or fracture (Fig. 2B). In contrast, the molar teeth of *Pvrl1*$^{-/-}$ mice appeared grossly normal (Fig. 2C and D). Scanning electron microscopy of the mature, erupted enamel revealed the normal 'herring-bone' pattern of prisms in the incisor teeth of wild-type mice (Fig. 2E); in contrast, the prismatic structure of the enamel of the incisor teeth of *Pvrl1*$^{-/-}$ mice was substantially less distinct (Fig. 2F).

The enamel of *Pvrl1*$^{-/-}$ incisor teeth is hypomineralized while the expression pattern of enamel matrix proteins is normal

Micro-radiographic analysis of the mature and maturation stage enamel of the lower incisor teeth revealed a statistically significant hypomineralization of *Pvrl1*$^{-/-}$ enamel (Fig. 3A). In contrast, the enamel in the secretory zone showed no statistically significant difference in mineral density (Fig. 3A), whereas the final enamel thickness was identical in both wild-type and *Pvrl1*$^{-/-}$ mice (Fig. 3B and C).

SDS–PAGE analysis (Fig. 4A) showed the protein composition of secretory stage wild-type and *Pvrl1*$^{-/-}$ developing enamel matrix to be identical. The apparent difference in protein content in the early maturation stage enamel is due to unavoidable sampling errors in delineating the start of the early maturation stage from the protein-rich, adjacent secretory stage enamel. In both wild-type and *Pvrl1*$^{-/-}$ samples, it is clear that matrix protein is largely removed from the tissue by the late maturation stage. Consistent with the western blot analysis, immunohistochemical analysis of the enamel extracellular matrix proteins amelogenin, ameloblastin and enamelin of wild-type and *Pvrl1*$^{-/-}$ mice showed identical staining patterns (Fig. 4B–G).

Maturation stage ameloblasts of *Pvrl1*$^{-/-}$ mice detach from the SI

Histological analysis was performed for the lower incisor teeth of 2–3-month-old wild-type and *Pvrl1*$^{-/-}$ mice (Fig. 5A). In wild-type mice, the normal cellular components of the enamel organ were evident (Fig. 5B–E). Identical structural components were present in the *Pvrl1*$^{-/-}$ lower incisor teeth (Fig. 5F and G); however, after commencement of the maturation zone, separation between the ameloblasts and the SI was evident (Fig. 5H and I). Separation began a short distance after the start of the maturation zone (typically 600–700 μm)

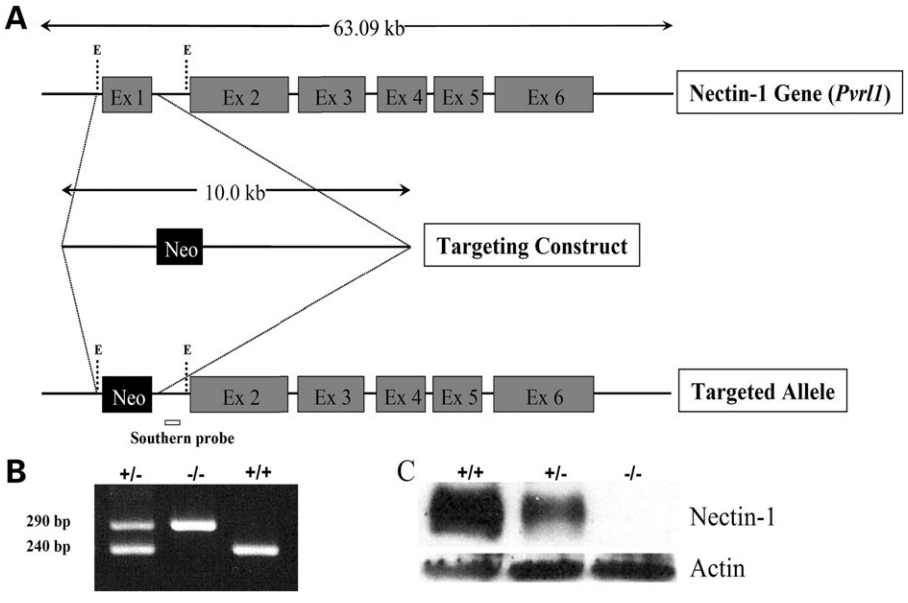

Figure 1. Generation of *Pvrl1*$^{-/-}$ mice. (**A**) Structure of *Pvrl1*, gene targeting vector and targeted allele following homologous recombination. Exons are depicted as grey boxes, whereas the neomycin-resistance cassette (neo) is shown as a black box. The *Eco*R1 sites used for cloning, E, and the position of the probe used for Southern blot analysis are also shown. (**B**) Confirmation of the genotypes of wild-type (+/+), heterozygous (±) and homozygous mutant (−/−) mice by duplex PCR analysis in which the wild-type and targeted alleles are represented by 240 and 290 bp products, respectively. (**C**) Western blot analysis of protein extracts from wild-type (+/+), heterozygous (±) and homozygous mutant (−/−) mouse embryos. No nectin-1 protein was detected in samples obtained from *Pvrl1*$^{-/-}$ embryos. Actin-1 loading controls are also shown.

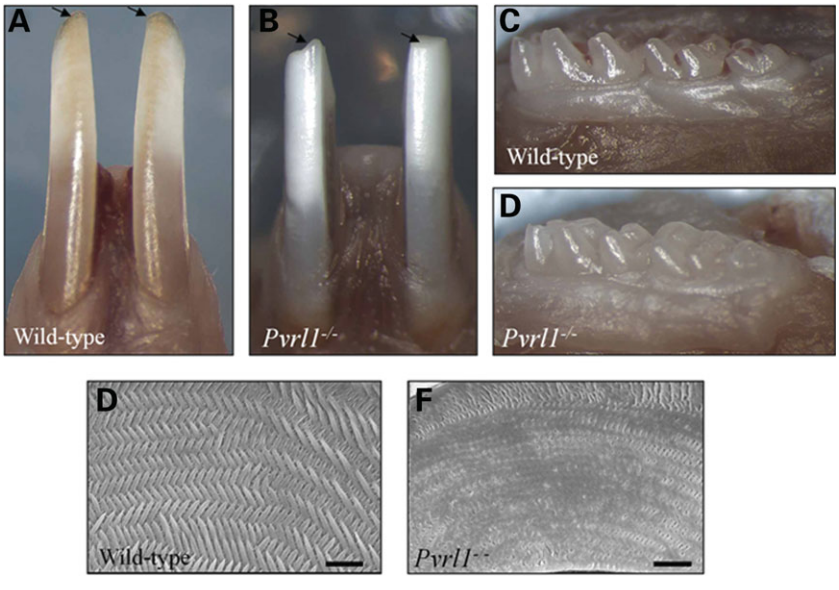

Figure 2. Morphology of the dentition of *Pvrl1*$^{-/-}$ mice. (**A**) The lower incisor teeth of wild-type mice are stained yellow and show a sharp incisal edge (arrows), whereas (**B**) the lower incisor teeth of *Pvrl1*$^{-/-}$ mice are chalky white in colour and often show signs of mechanical attrition and/or fracture (arrows). In contrast, the molar teeth of the wild-type (**C**) and *Pvrl1*$^{-/-}$ mice (**D**) appear grossly normal. (**E** and **F**) Scanning electron microscopy reveals that the normal 'herring-bone' pattern of hydroxyapatite prisms of the wild-type incisor (E) is absent from the *Pvrl1*$^{-/-}$ incisor (F). Scale bars, 10 μm.

as a split between the two cell layers (Fig. 5J), and developed more distally into a large blister-like structure (Fig. 5K). Where splitting had occurred, the maturation stage ameloblasts lost their columnar structure and adopted a cuboidal shape, similar to that of the post-maturation ameloblasts (Fig. 5L).

Loss of nectin-1 at the SI–ameloblast interface correlates with greatly reduced desmoplakin staining

Given the separation observed between the ameloblasts and the SI/papillary layer, the expression patterns of a series of cell–cell adhesion molecules were examined. (N.B. The

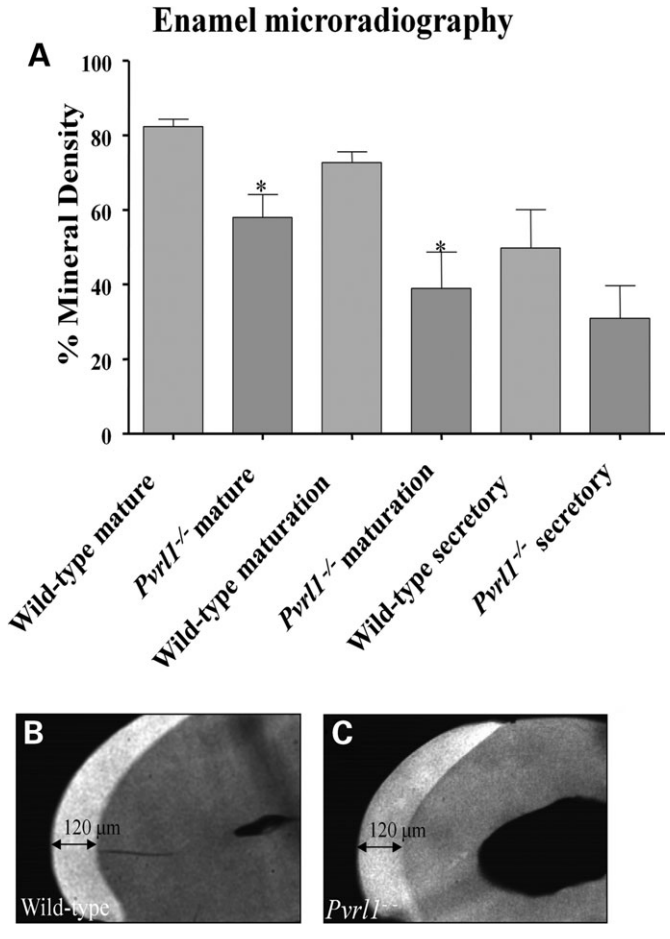

Figure 3. Micro-radiography and thickness of *Pvrl1*$^{-/-}$ enamel. (**A**) Micro-densitometric analysis of wild-type and *Pvrl1*$^{-/-}$ enamel revealed statistically significant differences ($P < 0.05$; asterisks) in mineral density between mature and maturation stage enamel. No statistically significant difference in mineral density was observed at the secretory stage of enamel formation. (**B** and **C**) Comparison of the thickness of mature enamel showed no differences between (B) wild-type and (C) *Pvrl1*$^{-/-}$ lower incisor teeth.

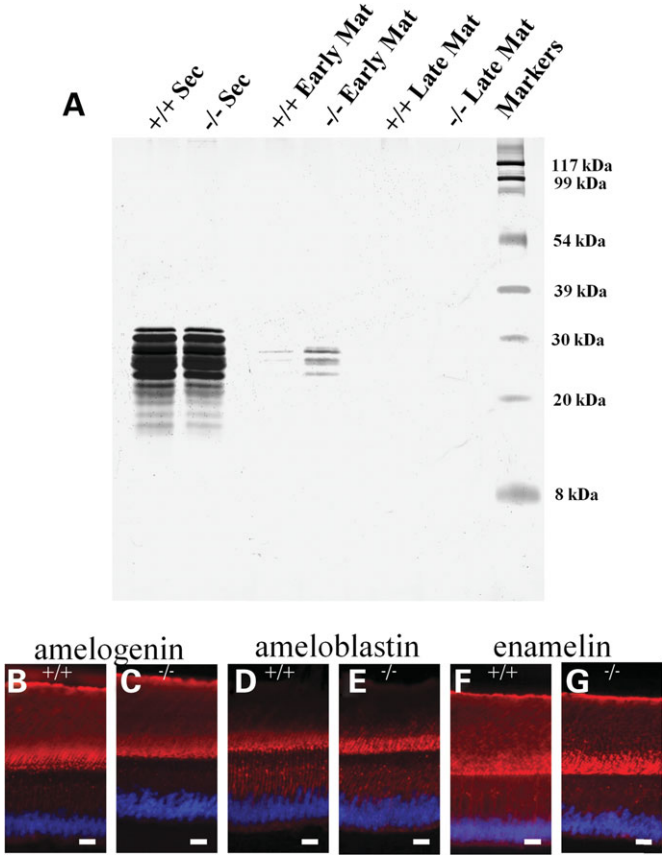

Figure 4. Biochemical and immunohistochemical analysis of the enamel extracellular matrix. (**A**) SDS–PAGE analysis of whole enamel extracts from the lower incisor teeth showed identical protein profiles between the secretory stage enamel of wild-type (+/+) and *Pvrl1*$^{-/-}$ (−/−) mice. In the early maturation stage enamel, the total protein content is much reduced in both wild-type and *Pvrl1*$^{-/-}$ lower incisor teeth. The differences in intensity between the wild-type and *Pvrl1*$^{-/-}$ samples at this stage of amelogenesis reflect the difficulty in sampling this region of the lower incisor. No enamel proteins were detected in the late maturation stage enamel of wild-type and *Pvrl1*$^{-/-}$ samples. (**B**–**G**) Immunohistochemical analysis of the major extracellular matrix proteins amelogenin (B, C), ameloblastin (D, E) and enamelin (F, G) showed no discernable differences between wild-type and *Pvrl1*$^{-/-}$ lower incisor teeth. Scale bars, 25 μm.

staining of the maturation zone of the *Pvrl1*$^{-/-}$ mouse described in this section relates to the short region that precedes the separation.) Immunostaining for nectin-1 was prominent in the secretory and maturation zones of wild-type mice but, consistent with the null genotype, was completely absent from the enamel organ of *Pvrl1*$^{-/-}$ mice (Fig. 6A–D). Staining also revealed a striking change in the pattern of nectin-1 distribution between the secretory and maturation zones. In the secretory zone, nectin-1 appeared to be concentrated at the apico-lateral margins of the ameloblasts (Fig. 6A) consistent with location to adherens junctions, with weaker staining along the entire lateral margins of the cells. Nectin-1 staining was also prominent in the SI where it is entirely surrounded the cells, including a punctate distribution at the SI–ameloblast interface (Fig. 6A, arrowhead). In the maturation zone, nectin-1 staining was similarly distributed on the lateral aspects of the shortened ameloblasts but strikingly concentrated at the SI-ameloblast interface (Fig. 6C, arrowhead), while staining on the lateral and basal surface of the SI cells was much reduced. Rather weak staining was present around the peripheries of the cells in the papillary layer.

Staining for the major adherens junction component β-catenin was generally very similar to the distribution of nectin-1, including a prominent adherens junction-like concentration at the apico-lateral margins of ameloblasts (Fig. 6E and G); however, one clear difference between the distributions of β-catenin and nectin-1 was that the former was not concentrated at the SI–ameloblast interface in the maturation zone (Fig. 6G, arrowhead). The distribution of β-catenin appeared completely unaffected in the *Pvrl1*$^{-/-}$ enamel organ (Fig. 6F and H).

The tight junction transmembrane protein occludin showed a prominent apico-lateral distribution between ameloblasts of both the secretory and maturation zones, consistent with the presence of tight junctions at this location (Fig. 6I and K). Similar but weaker staining at the proximal end of the amelo-

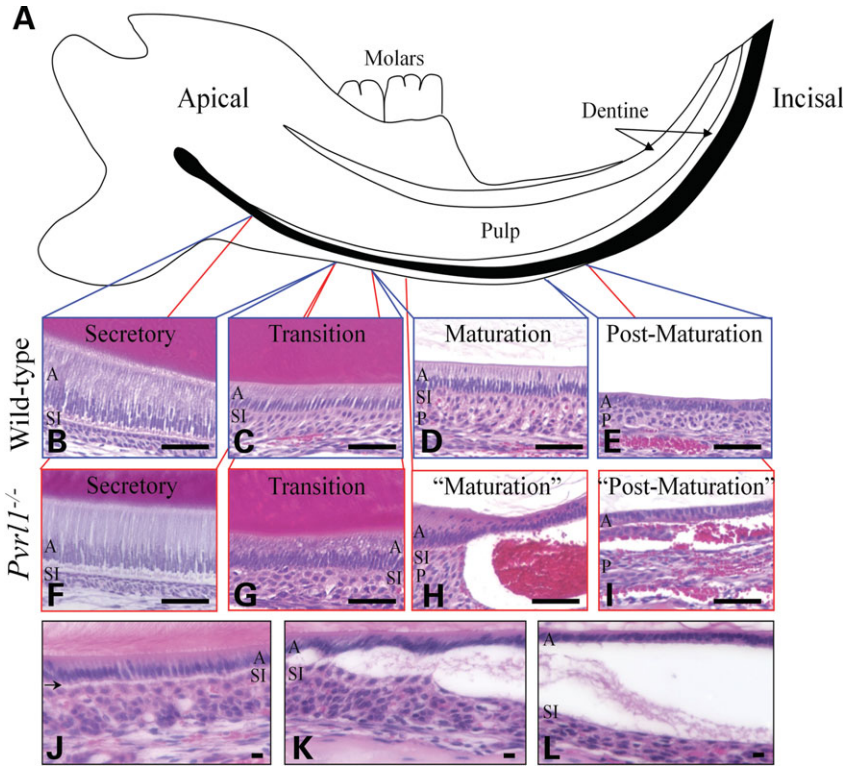

Figure 5. Histological analysis of the lower incisor teeth. (**A**) Diagrammatic representation of the mouse lower incisor tooth within the mandible. Amelogenesis commences at the apical region of the tooth and proceeds towards the incisal edge. The position of the regions concerned with enamel formation is shown in black. (**B**–**I**) The secretory (B), transition (C), maturation (D) and post-maturation (E) stages of amelogenesis showed characteristically normal morphology in the wild-type lower incisor. In the *Pvrl1*$^{-/-}$ lower incisor the secretory (F) and transition (G) stages also show normal morphology; however, the maturation (H) and post-maturation (I) stages show a separation between the ameloblasts and stratum intermedium forming a blister-like structure. (**J**–**L**) Separation of the ameloblasts from the stratum intermedium (arrow) begins soon after the start of the maturation stage (J), and worsens progressively in the incisal direction (K). Once a blister-like structure has formed (L), the ameloblasts lose their columnar morphology and adopt a cuboidal shape reminiscent of post-maturation ameloblasts. A, ameloblasts; SI, stratum intermedium; P, papillary layer. Scale bars: (A–I), 50 μm; (J–L), 10 μm.

blasts, adjacent to the SI, indicated the presence of less well-developed tight junctions in this region. Occludin distribution appeared unaffected in *Pvrl1*$^{-/-}$ mice (Fig. 6J and L).

Like nectin-1, the desmosomal plaque protein desmoplakin showed distinctly different distributions between the secretory and maturation zones of wild-type mice. In the secretory zone, desmoplakin staining was most prominent in the SI being strongly represented at the cell–cell boundaries with comparatively weak punctate staining of the SI–ameloblast interface (Fig. 6M). Desmoplakin staining between ameloblasts was weak but showed an apico-lateral component consistent with a contribution of desmosomes to the junctional complex in this region (Fig. 6M). In the maturation zone, desmoplakin staining was prominent at the SI–ameloblast interface and greatly reduced on the baso-lateral aspect of the SI cells, similar to the distribution of nectin-1 (Fig. 6O, arrowhead and compare with Fig. 6C). Desmoplakin distribution appeared to be unaffected in the secretory zone of *Pvrl1*$^{-/-}$ mice (Fig. 6N). In contrast, a great reduction of desmoplakin staining was evident at the SI–ameloblast interface of *Pvrl1*$^{-/-}$ mice (Fig. 6P, arrowhead). Bright fluorescence was also seen in the papillary layer of the *Pvrl1*$^{-/-}$ maturation zone (Fig. 6P, arrows) but this was an artefact owing to the presence of autofluorescent erythrocytes.

Desmosomes are fewer and smaller at the SI–ameloblast interface in the *Pvrl1*$^{-/-}$ enamel organ

In view of the loss of cell adhesion and the differences in desmoplakin immunostaining between wild-type and *Pvrl1*$^{-/-}$ mice, cell contact and, in particular, those desmosomes at the SI–ameloblast interface were examined ultrastructurally. In the secretory zone, there appeared to be a slight reduction in intercellular contact at the SI–ameloblast interface in *Pvrl1*$^{-/-}$ animals (Fig. 7A and B) whereas in the early maturation zone the degree of intercellular contact was greatly reduced compared with wild-type (Fig. 7C and D, red arrows). At higher magnification, the desmosomes in both regions and in both wild-type and null animals appeared to be normal in structure except that the intercellular structure of *Pvrl1*$^{-/-}$ desmosomes was less clearly defined (Fig. 7E–H). In addition, the desmosomes of the maturation zone of the incisor teeth of wild-type mice appeared larger and more abundant than those in the secretory zone, whereas those in both zones of *Pvrl1*$^{-/-}$ mice appeared smaller and fewer. These impressions were confirmed by quantification of desmosome number and size (Table 1); thus, there is an increase in desmosome size and number at the SI–ameloblast interface in wild-type mice and loss of nectin-1 caused *Pvrl1*$^{-/-}$ mice to have fewer, smaller desmosomes in this location.

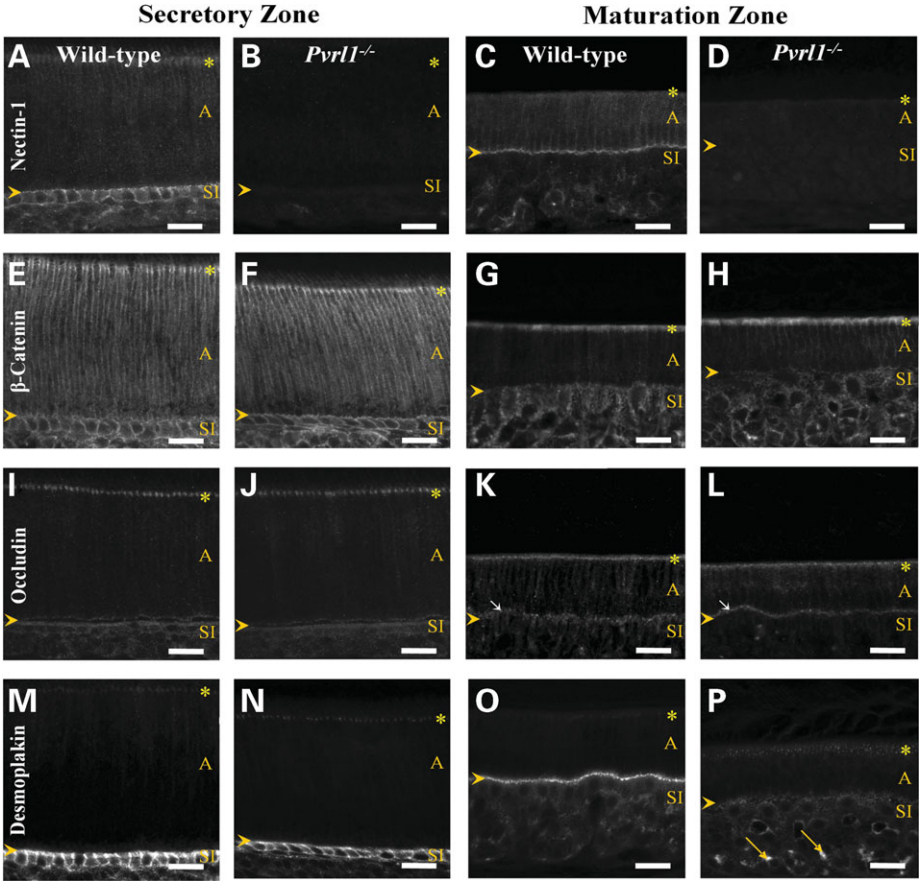

Figure 6. Immunohistochemical analysis of the lower incisor tooth. (**A**–**D**) Nectin-1 showed strong immunoreactivity around the cells of the stratum intermedium of the secretory zone and at the proximal junctional complex of the ameloblasts in wild-type mice (A). The immunoreactivity for nectin-1 shifted from around the stratum intermedium cells to the SI–ameloblast interface in the wild-type maturation zone (C). No nectin-1 expression was detected in the *Pvrl1*$^{-/-}$ secretory or maturation zones (B and D). (**E**–**F**) β-Catenin showed strong immunostaining of the stratum intermedium and ameloblast proximal junctional complexes of the secretory zone ameloblasts; moderate immunostaining for β-catenin was also seen between these ameloblasts in both wild-type and *Pvrl1*$^{-/-}$ mice (E and F). In the maturation zone, β-catenin expression appeared to decrease but remained strong at the proximal junctional complex of the ameloblast in both wild-type and *Pvrl1*$^{-/-}$ mice (G and H). (**I**–**L**) Occludin immunostaining in the secretory zone was similar in wild-type and *Pvrl1*$^{-/-}$ mice being strong at the ameloblast proximal junctional complex (I and J). In the maturation zone, occludin immunoreactivity was again similar between wild-type and *Pvrl1*$^{-/-}$ animals with strong labelling of the proximal and distal (arrows) junctional complexes of the ameloblasts (K and L). (**M**–**P**) Desmoplakin expression was strong at the SI–ameloblast interface in the secretory and maturation zones of wild-type mice (M and O). In *Pvrl1*$^{-/-}$ mice, however, strong expression was seen at the SI–ameloblast interface of the secretory zone but this was largely lost in the maturation zone (N and P). The yellow arrows indicate autofluorescence from erythrocytes, the yellow arrowheads mark the position of the SI–ameloblast interface and the yellow asterisks mark the position of the ameloblast proximal junctional complex. A, ameloblast, SI, stratum intermedium. Scale bar, 50 μm.

Absence of nectin-1 promotes cell proliferation but not apoptosis in the enamel organ

Loss of cell adhesion can trigger apoptosis (18). Ameloblasts of the incisor enamel organ are generated continuously from an apical progenitor cell population and, as they progress through the secretory and maturation zones, the numbers are reduced by ∼50% by apoptosis (15,19,20). To determine whether reduced cell adhesion resulting from the absence of nectin-1 led to increased apoptosis of ameloblasts TUNEL staining and immunofluorescence for activated caspase-3 were used. Clusters of TUNEL-positive and caspase-3-positive ameloblasts were present in the post-secretory transition zone of both wild-type and *Pvrl1*$^{-/-}$ mice with no obvious differences in the staining patterns between mice of either genotype (data not shown). No apoptotic ameloblasts were detected in the maturation zone of either group of animals but occasional TUNEL- and caspase-3-positive cells were present in the papillary layer of *Pvrl1*$^{-/-}$ mice (Fig. 8A and B); thus, the loss of nectin-1 promoted apoptosis in this region of the enamel organ.

The loss of cell adhesion may also affect the state of differentiation of cells causing a return to a more proliferative state. To investigate this possibility, wild-type and *Pvrl1*$^{-/-}$ mice were labelled with BrdU and their enamel organs examined. In both groups of mice, numerous BrdU-labelled nuclei were observed in the apical region of the lower incisor teeth from which undifferentiated ameloblasts arise continuously (data not shown). In contrast, once differentiation had occurred, BrdU-positive ameloblast nuclei were never observed in mice of either genotype (data not shown). In the maturation zone, papillary layer cells of wild-type mice contained occasional BrdU-positive nuclei (Fig. 8C) but the regions of

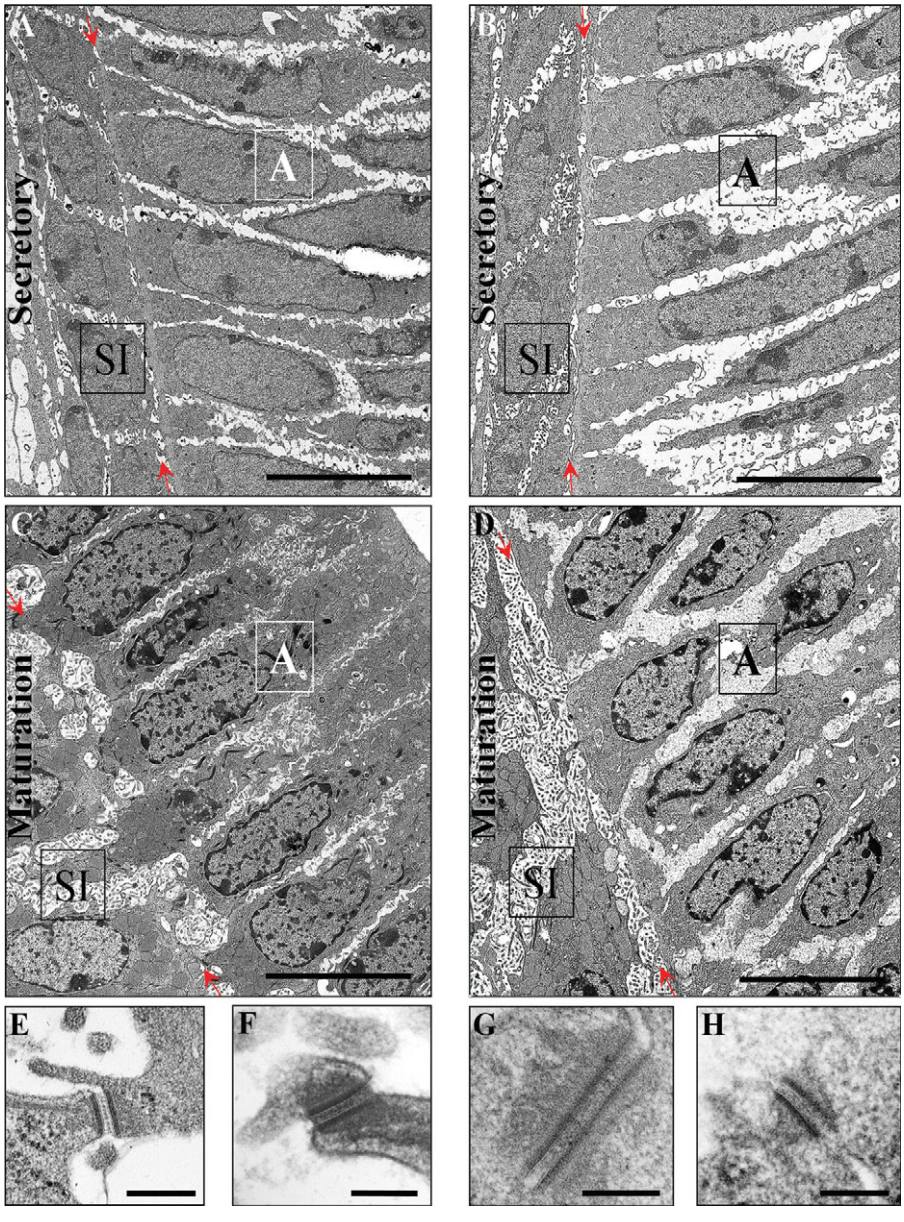

Figure 7. Transmission electron microscopy of the lower incisor enamel organ. (**A** and **B**) Low power electron micrographs of the secretory zone SI–ameloblast interface of (A) wild-type and (B) *Pvrl1*$^{-/-}$ mice. In both wild-type and *Pvrl1*$^{-/-}$ mice, there is close contact between the ameloblasts and stratum intermedium cells. (**C** and **D**) Low power electron micrographs of maturation zone SI–ameloblast interface of (C) wild-type and (D) *Pvrl1*$^{-/-}$ mice. In wild-type mice, numerous contacts are made between the stratum intermedium cells and the ameloblasts, whereas in the *Pvrl1*$^{-/-}$ mice little contact is made between these cells. The red arrows indicate the position of the SI–ameloblast interface. A, ameloblast, SI, stratum intermedium. Scale bars in A–D = 8 μm. (**E**–**H**) Examples of desmosomes seen at the SI–ameloblast interface in the secretory and maturation zones of wild-type and *Pvrl1*$^{-/-}$ mice. In the secretory zone of wild-type and *Pvrl1*$^{-/-}$ mice the desmosomes were of typical size (E and F, respectively). In contrast, while the desmosomes observed in the maturation zone of wild-type mice (G) were usually larger than those observed in the secretory zone, those observed in the maturation zone of *Pvrl1*$^{-/-}$ mice were of a similar size to those found in the secretory zone (H). Scale bar in: (E), 150 nm; (F–H), 160 nm.

Table 1. Comparison between desmosomes number and size at the SI–ameloblast interface of wild-type and *Pvrl1*$^{-/-}$ mice

	Secretory zone No/μm membrane	Size (nm)	Maturation zone No/μm membrane	Size (nm)
Wild-type	0.25 ± 0.02	202.0 ± 4.5	0.63 ± 0.07*	370.8 ± 8.8*
Pvrl1$^{-/-}$	0.08 ± 0.02**	184.1 ± 4.6**	0.10 ± 0.02**	231.0 ± 7.8**

All values are mean ± standard error for 200 desmosomes at each interface.
*Statistically significant difference between secretory zone and maturation zone ($P < 0.05$). **Statistically significant difference between wild-type and mutant ($P < 0.05$).

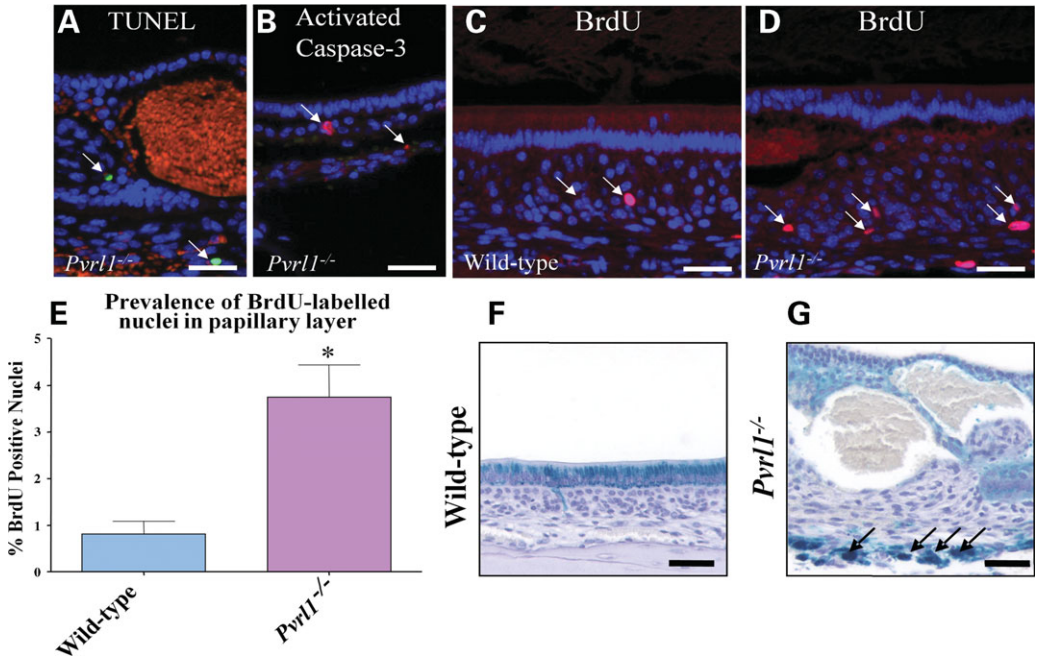

Figure 8. Apoptosis, proliferation and iron transport in *Pvrl1*$^{-/-}$ mice (**A** and **B**) Occasional TUNEL-positive nuclei (A), and activated caspase-3 positive cells (B), were observed in the papillary layer of *Pvrl1*$^{-/-}$ mice beneath the regions where ameloblast separation had occurred (arrows). Orange areas are artefactual and correspond to autofluorescence from erythrocytes. (**C**) Occasional BrdU-positive nuclei were observed in the papillary layer of wild-type mice (arrow). (**D**) BrdU-positive nuclei were more numerous in the papillary layer of *Pvrl1*$^{-/-}$ mice. (**E**) Quantitative analysis of the BrdU-positive nuclei in the papillary layer of wild-type and *Pvrl1*$^{-/-}$ mice indicated a statistically significant increase ($P < 0.05$) in the latter of ~3%. (**F**) Perl's Prussian blue reaction of wild-type maturation zone showed strong reactivity (blue) in a supra-nuclear position within the ameloblasts. (**G**) Similar preparation as (F), showing the maturation zone of a *Pvrl1*$^{-/-}$ mouse. Reactivity was not concentrated in the ameloblasts as it was in wild-type mice but remained diffuse throughout the whole layer. Above the vascular bed that underlies the enamel organ, cells showing strong reactivity were often seen (arrows). Scale bar in (A–D), (F) and (G) is 50 μm.

SI–ameloblast separation in *Pvrl1*$^{-/-}$ mice contained significantly more BrdU-positive cells (Fig. 8D and E), indicating that the loss of cell adhesion promoted cell proliferation.

Absence of nectin-1 impairs iron transport in the enamel organ

One-third of the way through the maturation stage, ameloblasts begin to accumulate supra-nuclear ferritin particles and, at the late maturation stage, they secrete iron onto the mature enamel surface just prior to eruption (16,17). As *Pvrl1*$^{-/-}$ mice showed the absence of enamel iron pigmentation, we used Perls' Prussian blue reaction to demonstrate ferric iron distribution in the enamel organs of wild-type and *Pvrl1*$^{-/-}$ mice. In wild-type and *Pvrl1*$^{-/-}$ mice, blue staining corresponding to ferric iron was present within the papillary layer as small particles and diffusely in the ameloblasts in the area where the enamel matrix is degraded. As maturation progressed, the iron pigment accumulated in the supra-nuclear region of wild-type ameloblasts as dark blue particles (Fig. 8F), whereas in the *Pvrl1*$^{-/-}$ ameloblasts, following separation, iron staining remained diffuse or absent (Fig. 8G). Furthermore, below the 'blistered' regions large, iron-laden cells, probably scavenging macrophages, were often present (Fig. 8G); thus iron transport in the enamel organ appears to be impeded in the absence of nectin-1 and this may reflect a general impairment of ion transport.

DISCUSSION

We have discovered a fundamental function of nectin-1 in the cell biology of amelogenesis in the mouse. The incisor teeth of *Pvrl1*$^{-/-}$ mice showed decreased iron pigmentation with increased wear and fragility consistent with hypomineralization. Histologically, *Pvrl1*$^{-/-}$ mice showed a foreshortened functional maturation zone because the ameloblasts at this developmental stage lost contact with the underlying papillary layer forming blister-like structures. This separation occurred along the SI–ameloblast boundary where intercellular adhesion appeared to be reduced as the result of loss of nectin-1 and a substantial reduction in the size and number of desmosomes.

Investigation of wild-type mice suggests that the SI–ameloblast interface in the maturation zone is specialized for strong intercellular adhesion. This region shows intense immunofluorescence for nectin-1 and, surprisingly, rather weak staining for β-catenin (elsewhere in the tissue, especially in the ameloblasts, nectin-1 and β-catenin shows very similar staining patterns suggesting co-localization to adherens junctions). The expression pattern of nectin-1 during post-natal incisor tooth development observed in the current study is entirely consistent with its expression at cell–cell contacts in the SI during the embryonic stages of tooth development (21). The abundance of nectin-1 at the SI–ameloblast interface of the incisor teeth is accompanied by a significant increase in the size and number of desmosomes compared with the

adjacent secretory zone. Desmosomes in tissues are generally hyper-adhesive to mediate strong intercellular binding (22–24). It seems likely that specialization for increased adhesiveness at the SI–ameloblast interface in the maturation zone is an adaptation to enable it to resist disruption by eruptive and masticatory forces. In consequence, the loss of nectin-1 and the reduction in desmosomes in the maturation zone of the incisors of *Pvrl1*$^{-/-}$ mice destroy the capacity to resist such forces and lead to splitting.

Nectin-1 has previously been reported to be an organizer and stabilizer of adherens junctions and tight junctions in epithelial junctional complexes (25–34). Our immunofluorescence studies indicate that the distribution of β-catenin and occludin were unaffected in the *Pvrl1*$^{-/-}$ enamel organ, suggesting that adherens and tight junctions were also unaffected. These junctions may be maintained by compensatory contribution from other members of the nectin family. In contrast, desmosomes were markedly reduced. The potential involvement of any of the members of the nectin family with desmosomal biology has not, to our knowledge, been reported previously and the mechanism of how nectin-1 is involved represents an exciting area for future investigation.

Our data provide valuable information in respect of maturation stage ameloblast function, the precise details of which remain obscure. The function of maturation stage ameloblasts is thought to be primarily one of the ion transport/regulations to facilitate secondary crystal growth, completing enamel mineralization to produce a hard, highly mineralized tissue (35). The papillary layer itself is also potentially active in ion transport during this stage (36) and this, together with the large number of junctional complexes between the two layers, has prompted the suggestion that they may act as a single functional unit during enamel maturation (37). The loss of attachment between the SI/papillary layer and the maturation stage ameloblasts as seen in the *Pvrl1*$^{-/-}$ incisors would be expected to result in a failure of ion transport, explaining the resulting enamel hypomineralization observed in these animals and further exemplified by the loss of iron pigmentation in these teeth. It has also been suggested that maturation stage ameloblasts are pro-active in absorbing protein from the enamel extracellular matrix (38), which is a pre-requisite for secondary crystal growth (39). Our results indicate that while secondary crystal growth was clearly impaired in the *Pvrl1*$^{-/-}$ incisors, firmly supporting the role of maturation stage ameloblasts and their association with the SI/papillary layer in ion transport, protein withdrawal appeared to be normal. This suggests that the removal of protein from the extracellular matrix is more likely to be one of the passive rather than active uptakes.

Premature adoption of cuboidal morphology by ameloblasts and increased proliferation in the papillary layer of the *Pvrl1*$^{-/-}$ enamel organ suggest that cellular differentiation may be affected by the loss of nectin-1. Further support for this hypothesis is provided by the observation that ameloblastin expression, which is usually high in maturation stage ameloblasts (40), declines substantially once contact with the SI is lost (Supplementary Material, Fig. S1). The signals driving the sequence of ameloblast differentiation from the secretory to the maturation stages are unknown. Our data from the analysis of *Pvrl1*$^{-/-}$ mice suggest that intimate association between ameloblasts and the underlying SI/papillary layer is key to maintain the differentiated maturation ameloblast phenotype. The loss of differentiation following separation from the SI/papillary layer observed in the *Pvrl1*$^{-/-}$ mice suggests that the signals required to maintain maturation-stage ameloblast function arise in the SI/papillary layer rather than as a feedback mechanism from the enamel itself, as suggested previously (41). There is accumulating evidence that desmosomal adhesion is important for maintaining cellular differentiation (42–44), so it is possible that the substantial alterations in desmosomal adhesion contribute to the differentiative changes that we have observed.

It is also possible that nectin-1 and desmosomal adhesion help to co-ordinate the movement of secretory ameloblast cohorts relative to one another. This co-ordinated movement delineates the characteristic prismatic structure of enamel. The loss of co-ordinated cell movement due to adhesive defects would be expected to result in abnormal prismatic structure in the mature tissue and would explain the unusual ultrastructural appearance of *Pvrl1*$^{-/-}$ enamel in the scanning electron microscope.

The molar teeth of *Pvrl1*$^{-/-}$ mice were unaffected and this may be because their enamel develops pre-eruption, which is before they are subject to the mechanical stresses associated with tooth eruption and mastication. Similarly, the enamel of the human dentition also develops pre-eruption and so although dental abnormalities such as small, missing or reduced numbers of teeth occur in Margarita Island ectodermal dysplasia, which is caused by a nonsense mutation in the *PVRL1* gene (12), defects of enamel formation have not been reported in this condition (45). Interestingly, *Pvrl1*$^{-/-}$ mice do not phenocopy their human counterparts in other respects; e.g. cleft lip/palate and hidrotic ectodermal dysplasia are not observed in *Pvrl1*$^{-/-}$ mice. These phenotypic differences may result from functional redundancy between nectin-1 and -3 in mice, which are not present in man.

In conclusion, we have shown for the first time that nectin-1 has a fundamental role in murine amelogenesis. The defect of amelogenesis is seen to be associated with a failure of adhesion at the SI–ameloblast boundary of the enamel organ accompanied by desmosomal deficits such as reduced prevalence and impaired biogenesis.

MATERIALS AND METHODS

Generation of *Pvrl1*$^{-/-}$ mice

A gene-targeting vector was generated by inserting a 3 kb *Xba*I–*Bam*HI fragment and a 5 kb *Cla*I–*Sal*I fragment from the 5′ end of the nectin-1 gene sequentially into the pBluescript II SK^{-} vector as 5′ and 3′ arms of homology, respectively. The region containing exon 1 of *Pvrl1*$^{-/-}$ was excised using *Eco*RI and replaced by a 1.8 kb genomic fragment containing a neomycin resistance cassette. The resulting construct was confirmed by sequence analysis.

The vector was linearized with *Sal*I and electroporated into R1 embryonic stem cells, which were cultured in DMEM containing G418 (500 μg/ml) to select for neomycin resistant clones. Correctly targeted clones were identified by Southern analysis using a 740 bp probe external to the neomycin

resistance cassette cloning site. In this way, wild-type and targeted alleles could be distinguished as 13 and 15 kb *Eco*RV fragments, respectively.

The targeted embryonic stem cells were injected into blastocysts derived from C57BL/6 mice and used to generate chimeric mice. Such mice were crossed onto a mixed genetic background to select for heterozygotes. Genotypes were confirmed by a duplex PCR assay (forward primer: 5′-AGC TGT TTC CGT CTG GTG TC-3′, wild-type reverse primer: 5′-AGG GGT GGA GTT AAG ATG AGG-3′, neomycin-resistance cassette reverse primer: 5′-CTT GGC TGG ACG TAA ACT CC-3′), which distinguished wild-type and targeted alleles as 290 and 240 bp bands, respectively.

To confirm that this approach resulted in a null allele, we performed western blot analysis using protein lysates prepared from 16 day post-coitum embryo heads. Lysates from wild-type, *Pvrl1*$^{\pm}$ and *Pvrl1*$^{-/-}$ embryos were resolved on 9% SDS–PAGE gels, transferred to nitrocellulose membranes (Bio-Rad) and immunoblotted using antibodies to nectin-1 (H62; Santa Cruz) and actin-1 (Sigma-Aldrich). Immune complexes were detected using horseradish peroxidise-conjugated secondary antibodies followed by enhanced chemiluminescence (Amersham Biosciences). All procedures were performed in accordance with the UK Animals (Scientific Procedures) Act of 1986.

Preparation of teeth for micro-radiography and scanning electron microscopy

Lower incisors were dissected from the jaws of four 2--month-old wild-type and four 2-month-old *Pvrl1*$^{-/-}$ mice, freeze dried and embedded in methyl methacrylate, adhering soft tissue having been removed. The embedded teeth were then sectioned transverse to the long axis of the tooth using an Accutom-5 cutter with a peripheral diamond cutting disc and minimal water cooling to minimize the loss of water soluble components within the enamel. Sections were taken at points corresponding to the end of secretion, maturation and fully mature enamel and polished plano-parallel with 1200 grade carborundum paper to a thickness of approximately $\sim$100 μm (final thickness being determined by micrometer measurement) then acid etched for exactly 15 s with 35% phosphoric acid to remove the smear layer and thoroughly washed in distilled water (pH 7.0).

Mineral density measurements

Mineral density across the full thickness of enamel within the sections was determined by transverse microradiography (TMR). Sections were contact microradiographed (6 min) on Kodak High Resolution plate, type 1A, by Ni-filtered Cu-K radiation at 20 kV, 4 mA. An aluminium step wedge was included to permit the quantification. The microradiographs were developed in Kodak HRP developer and then analysed by TMRW software (version 20.0.27.16, 2000) (Inspektor Research Systems, Amsterdam, The Netherlands). The enhanced images of the microradiographs were analysed under standard conditions of light intensity and magnification and were processed, along with data from measurement of the aluminium step wedge, by TMR. Micro-radiographic measurements were analysed using graphical software (Graphpad Prism, San Diego, CA, USA), and a two-tailed Mann–Whitney *U* test was performed for significance.

Scanning electron microscopy

Following the micro-radiography, the sections were mounted on aluminium stubs and sputter coated with gold. Microstructural analysis was undertaken using a Jeol 35 SEM fitted with the Deben 'Genie' upgrade (Deben Engineering, Debenham, UK).

SDS–PAGE analysis

Four 2-month-old wild-type and four 2-month-old *Pvrl1*$^{-/-}$ mice were killed by cervical dislocation and the mandibles removed. The contralateral incisors were dissected free of the mandibular bone and the enamel organs carefully wiped away with moist tissue paper. After $\sim$1 min, the white opaque zone indicative of the maturation stage became apparent. Contiguous samples of secretory, early maturation and late maturation stage enamel were micro-dissected clear of the dentine using a scalpel. All samples were stored at -80°C.

For total protein analysis, the enamel samples from both contralateral incisors were dissolved in 20 μl of 10% acetic acid. Once dissolved, 180 μl of SDS sample-loading buffer was added and the samples were neutralized by addition of 7.5 μl of 5 M NaOH. Samples were loaded at 10 μl per lane and subjected to mini gel electrophoresis (Bio- Rad protean III) using 15% Tris/glycine gels run at a constant 200 V. Resolved proteins were visualized by silver staining.

Histological analysis

Mandibles from 2-month-old mice (10 wild-type and 10 *Pvrl1*$^{-/-}$) were dissected following cervical dislocation and fixed in neutral buffered formalin at room temperature for 48 h. Following fixation, the mandibles were decalcified in 5% EDTA, dehydrated through a graded ethanol series, cleared in chloroform, embedded as hemi-mandibles in paraffin wax, sectioned and stained with haematoxylin and eosin, or Perls' Prussian blue reaction according to standard methods (46). Sections were examined using a DMRB microscope (Leica) and Spot^{TM} digital camera and associated software (RTKE/SE Diagnostic Instruments Inc.).

Immunohistochemistry and TUNEL assay

Immunohistochemical analysis was performed on 2-month-old mandibles prepared as described above (four wild-type and four *Pvrl1*$^{-/-}$), using antibodies raised against nectin-1 (H-62, Santa Cruz), β-catenin (Sigma), desmoplakin (11-5F, D. Garrod), occludin (Zymed), activated caspase 3 (Abcam), amelogenin (Santa Cruz), ameloblastin (Santa Cruz) and enamelin (J. Kirkham). Primary antibodies were detected using biotinylated secondary antibodies (Vector laboratories) followed by Cy-3-conjugated streptavidin (Sigma) and mounted in fluorescence mountant containing DAPI (Vector laboratories). The TUNEL assay was performed according to

the manufacturer's instructions (Roche Diagnostics). Sections were examined as described above.

Transmission electron microscopy

Two-month-old mouse mandibles (four wild-type and four *Pvrl1*$^{-/-}$) were dissected following cervical dislocation and fixed in 2% paraformaldehyde/2% glutaraldehyde prepared in 0.1 M cacodylate buffer containing 0.15 M sucrose and 2 mM calcium chloride (pH 7.3) at 4°C overnight. Hemimandibles were decalcified for 2 weeks as described above and dissected axially into posterior, medial and anterior sections. Following dissection, the samples were washed with cacodylate buffer, post-fixed in 1% osmium tetroxide, dehydrated through a graded ethanol series, cleared in propylene oxide and embedded in 100 resin (Agar Scientific Ltd). Ultrathin sections were contrasted with uranyl acetate and lead citrate, and examined on a Philips model 400 transmission electron microscope.

A comparison was made of the numbers of desmosomes at the SI–ameloblast interface in four wild-type and four *Pvrl1* $^{-/-}$ animals. Non-overlapping, contiguous electron micrographs were taken of equivalent maturation zone regions in all mice. Desmosomes found to fall on the SI–ameloblast boundary were enumerated, and the number of desmosomes per micrometre length was calculated. The distribution of desmosome sizes was also obtained by measuring all desmosomes present in the same images. These values were analysed using graphical software (Graphpad Prism), and a two-tailed Mann–Whitney test was performed for significance.

Cell proliferation assay

Cell proliferation was detected by intraperitoneal injection of BrdU-labelling reagent (Amersham Biosciences) at 100 μg/g body weight into four 2-month-old wild-type and four 2--month-old *Pvrl1* $^{-/-}$ mice. The mice were killed by cervical dislocation 2 h later and their mandibles were processed as for histological analysis. Sections were immunolabelled using an antibody to BrdU (Abcam) following retrieval in 10 mM sodium citrate (pH 6.0) and detected using a biotinylated secondary antibody (Vector laboratories) and Cy3-conjugated streptavidin (Sigma).

Sufficient images were collected, from identical regions of each specimen, to allow a minimum of 400 nuclei to be counted. The percentage of BrdU-positive nuclei was then calculated and analysed using graphical software (Graphpad Prism) and a two-tailed Mann–Whitney test was performed for significance.

SUPPLEMENTARY MATERIAL

Supplementary Material is available at *HMG* Online.

FUNDING

This work was supported by the Wellcome Trust (066173, 075945). Funding to Pay the Open Access Charge was provided by the Wellcome Trust.

ACKNOWLEDGEMENTS

We thank Professor Helen Worthington (Faculty of Medial and Human Sciences, University of Manchester) for statistical advice, Charlotte Hunt (Faculty of Life Sciences, University of Manchester) and Sarah Myers (Oral Biology, University of Leeds) for expert technical assistance. We also thank Samantha Forbes of the electron microscopic service in the Faculty of Life Sciences, University of Manchester, for her help with the transmission electron microscopy.

Conflict of Interest statement. None declared.

REFERENCES

1. Miyoshi, J. and Takai, Y. (2007) Nectin and nectin-like molecules: biology and pathology. *Am. J. Nephrol.*, **27**, 590–604.
2. Ogita, H. and Takai, Y. (2006) Nectins and nectin-like molecules: roles in cell adhesion, polarization, movement, and proliferation. *I.U.B.M.B. Life*, **58**, 334–343.
3. Satoh-Horikawa, K., Nakanishi, H., Takahashi, K., Miyahara, M., Nishimura, M., Tachibana, K., Mizoguchi, A. and Takai, Y. (2000) Nectin-3, a new member of immunoglobulin-like cell adhesion molecules that shows homophilic and heterophilic cell–cell adhesion activities. *J. Biol. Chem.*, **275**, 10291–10299.
4. Mandai, K., Nakanishi, H., Satoh, A., Obaishi, H., Wada, M., Nishioka, H., Itoh, M., Mizoguchi, A., Aoki, T., Fujimoto, T. *et al.* (1997) Afadin: A novel actin filament-binding protein with one PDZ domain localized at cadherin-based cell-to-cell adherens junction. *J. Cell Biol.*, **139**, 517–528.
5. Takai, Y. and Nakanishi, H. (2003) Nectin and afadin: novel organizers of intercellular junctions. *J. Cell Sci.*, **116**, 17–27.
6. Ikeda, W., Nakanishi, H., Miyoshi, J., Mandai, K., Ishizaki, H., Tanaka, M., Togawa, A., Takahashi, K., Nishioka, H., Yoshida, H. *et al.* (1999) Afadin: A key molecule essential for structural organization of cell–cell junctions of polarized epithelia during embryogenesis. *J. Cell Biol.*, **146**, 1117–1132.
7. Mueller, S., Rosenquist, T.A., Takai, Y., Bronson, R.A. and Wimmer, E. (2003) Loss of nectin-2 at Sertoli-spermatid junctions leads to male infertility and correlates with severe spermatozoan head and midpiece malformation, impaired binding to the zona pellucida, and oocyte penetration. *Biol. Reprod.*, **69**, 1330–1340.
8. Inagaki, M., Irie, K., Ishizaki, H., Tanaka-Okamoto, M., Miyoshi, J. and Takai, Y. (2006) Role of cell adhesion molecule nectin-3 in spermatid development. *Genes Cells*, **11**, 1125–1132.
9. Inagaki, M., Irie, K., Ishizaki, H., Tanaka-Okamoto, M., Morimoto, K., Inoue, E., Ohtsuka, T., Miyoshi, J. and Takai, Y. (2005) Roles of cell-adhesion molecules nectin 1 and nectin 3 in ciliary body development. *Development*, **132**, 1525–1537.
10. Honda, T., Sakisaka, T., Yamada, T., Kumazawa, N., Hoshino, T., Kajita, M., Kayahara, T., Ishizaki, H., Tanaka-Okamoto, M., Mizoguchi, A. *et al.* (2006) Involvement of nectins in the formation of puncta adherentia junctions and the mossy fiber trajectory in the mouse hippocampus. *Mol. Cell Neurosci.*, **31**, 315–325.
11. Togashi, H., Miyoshi, J., Honda, T., Sakisaka, T., Takai, Y. and Takeichi, M. (2006) Interneurite affinity is regulated by heterophilic nectin interactions in concert with the cadherin machinery. *J. Cell Biol.*, **174**, 141–151.
12. Suzuki, K., Hu, D., Bustos, T., Zlotogora, J., Richieri-Costa, A., Helms, J.A. and Spritz, R.A. (2000) Mutations of PVRL1, encoding a cell–cell adhesion molecule/herpesvirus receptor, in cleft lip/palate-ectodermal dysplasia. *Nat. Genet.*, **25**, 427–430.
13. Sozen, M.A., Suzuki, K., Tolarova, M.M., Bustos, T., Fernandez Iglesias, J.E. and Spritz, R.A. (2001) Mutation of PVRL1 is associated with sporadic, non-syndromic cleft lip/palate in northern Venezuela. *Nat. Genet.*, **29**, 141–142.
14. Hay, M.F. (1961) The development in vivo and in vitro of the lower incisor and molars of the mouse. *Arch. Oral Biol.*, **3**, 86–109.

15. Smith, C.E. and Warshawsky, H. (1975) Cellular renewal in the enamel organ and the odontoblast layer of the rat incisor as followed by radioautography using 3H-thymidine. *Anat. Rec.*, **183**, 523–561.
16. Halse, A. (1972) Location and first appearance of rat incisor pigmentation. *Scand. J. Dent. Res.*, **80**, 428–433.
17. Kallenbach, E. (1970) Fine structure of rat incisor enamel organ during late pigmentation and regression stages. *J. Ultrastruct. Res.*, **30**, 38–63.
18. Frisch, S.M. and Francis, H. (1994) Disruption of epithelial cell–matrix interactions induces apoptosis. *J. Cell Biol.*, **124**, 619–626.
19. Ohshima, H., Nakasone, N., Hashimoto, E., Sakai, H., Nakakura-Ohshima, K. and Harada, H. (2005) The eternal tooth germ is formed at the apical end of continuously growing teeth. *Arch. Oral Biol.*, **50**, 153–157.
20. Smith, C.E. and Warshawsky, H. (1977) Quantitative analysis of cell turnover in the enamel organ of the rat incisor. Evidence for ameloblast death immediately after enamel matrix secretion. *Anat. Rec.*, **187**, 63–98.
21. Okabe, N., Ozaki-Kuroda, K., Nakanishi, H., Shimizu, K. and Takai, Y. (2004) Expression patterns of nectins and afadin during epithelial remodeling in the mouse embryo. *Dev. Dyn.*, **230**, 174–186.
22. Garrod, D.R., Berika, M.Y., Bardsley, W.F., Holmes, D. and Tabernero, L. (2005) Hyper-adhesion in desmosomes: its regulation in wound healing and possible relationship to cadherin crystal structure. *J. Cell Sci.*, **118**, 5743–5754.
23. Kimura, T.E., Merritt, A.J. and Garrod, D.R. (2007) Calcium-independent desmosomes of keratinocytes are hyper-adhesive. *J. Invest. Dermatol.*, **127**, 775–781.
24. Garrod, D. and Chidgey, M. (2008) Desmosome structure, composition and function. *Biochim. Biophys. Acta*, **1778**, 572–587.
25. Fukuhara, A., Irie, K., Nakanishi, H., Takekuni, K., Kawakatsu, T., Ikeda, W., Yamada, A., Katata, T., Honda, T., Sato, T. *et al.* (2002) Involvement of nectin in the localization of junctional adhesion molecule at tight junctions. *Oncogene*, **21**, 7642–7655.
26. Fukuhara, A., Irie, K., Yamada, A., Katata, T., Honda, T., Shimizu, K., Nakanishi, H. and Takai, Y. (2002) Role of nectin in organization of tight junctions in epithelial cells. *Genes Cells*, **7**, 1059–1072.
27. Fukuhara, T., Shimizu, K., Kawakatsu, T., Fukuyama, T., Minami, Y., Honda, T., Hoshino, T., Yamada, T., Ogita, H., Okada, M. *et al.* (2004) Activation of Cdc42 by trans interactions of the cell adhesion molecules nectins through c-Src and Cdc42-GEF FRG. *J. Cell Biol.*, **166**, 393–405.
28. Hoshino, T., Sakisaka, T., Baba, T., Yamada, T., Kimura, T. and Takai, Y. (2005) Regulation of E-cadherin endocytosis by nectin through afadin, Rap1 and p120ctn. *J. Biol. Chem.*, **280**, 24095–24103.
29. Kawakatsu, T., Ogita, H., Fukuhara, T., Fukuyama, T., Minami, Y., Shimizu, K. and Takai, Y. (2005) Vav2 as a Rac-GDP/GTP exchange factor responsible for the nectin-induced, c-Src- and Cdc42-mediated activation of Rac. *J. Biol. Chem.*, **280**, 4940–4947.
30. Ooshio, T., Fujita, N., Yamada, A., Sato, T., Kitagawa, Y., Okamoto, R., Nakata, S., Miki, A., Irie, K. and Takai, Y. (2007) Cooperative roles of Par-3 and afadin in the formation of adherens and tight junctions. *J. Cell Sci.*, **120**, 2352–2365.
31. Sato, T., Fujita, N., Yamada, A., Ooshio, T., Okamoto, R., Irie, K. and Takai, Y. (2006) Regulation of the assembly and adhesion activity of E-cadherin by nectin and afadin for the formation of adherens junctions in Madin–Darby canine kidney cells. *J. Biol. Chem.*, **281**, 5288–5299.
32. Takai, Y., Sasaki, T. and Matozaki, T. (2001) Small GTP-binding proteins. *Physiol. Rev.*, **81**, 153–208.
33. Takenawa, T. and Miki, H. (2001) WASP and WAVE family proteins: key molecules for rapid rearrangement of cortical actin filaments and cell movement. *J. Cell Sci.*, **114**, 1801–1809.
34. Yamada, A., Fujita, N., Sato, T., Okamoto, R., Ooshio, T., Hirota, T., Morimoto, K., Irie, K. and Takai, Y. (2006) Requirement of nectin, but not cadherin, for formation of claudin-based tight junctions in annexin II-knockdown MDCK cells. *Oncogene*, **25**, 5085–5102.
35. Smith, C.E. (1998) Cellular and chemical events during enamel maturation. *Crit. Rev. Oral Biol. Med.*, **9**, 128–161.
36. Garant, P.R., Sasaki, T. and Colflesh, P.E. (1987) Na-K-ATPase in the enamel organ: localization and possible roles in enamel formation. *Adv. Dent. Res.*, **1**, 267–275.
37. Skobe, Z., Stern, D.N. and Prostak, K.S. (1995) The cell biology of amelogenesis. Robinson, C., Kirkham, J. and Shore, R. (eds), *Dental Enamel; Formation to Destruction.*, CRC Press, Boca Raton, pp. 23–57.
38. Zou, Y., Wang, H., Shapiro, J.L., Okamoto, C.T., Brookes, S.J., Lyngstadaas, S.P., Snead, M.L. and Paine, M.L. (2007) Determination of protein regions responsible for interactions of amelogenin with CD63 and LAMP1. *Biochem. J.*, **408**, 347–354.
39. Robinson, C., Kirkham, J., Stonehouse, N.J. and Shore, R.C. (1989) Control of crystal growth during enamel maturation. *Connect. Tissue Res.*, **22**, 139–145.
40. Lee, S.K., Krebsbach, P.H., Matsuki, Y., Nanci, A., Yamada, K.M. and Yamada, Y. (1996) Ameloblastin expression in rat incisors and human tooth germs. *Int. J. Dev. Biol.*, **40**, 1141–1150.
41. Fincham, A.G. and Simmer, J.P. (1997) Amelogenin proteins of developing dental enamel. *Ciba Found. Symp.*, **205**, 118–130. Discussion 130–134.
42. Dusek, R.L., Godsel, L.M. and Green, K.J. (2007) Discriminating roles of desmosomal cadherins: beyond desmosomal adhesion. *J. Dermatol. Sci.*, **45**, 7–21.
43. Garrod, D.R., Merritt, A.J. and Nie, Z. (2002) Desmosomal cadherins. *Curr. Opin. Cell Biol.*, **14**, 537–545.
44. Getsios, S., Huen, A.C. and Green, K.J. (2004) Working out the strength and flexibility of desmosomes. *Nat. Rev. Mol. Cell Biol.*, **5**, 271–281.
45. Bustos, T., Simosa, V., Pinto-Cisternas, J., Abramovits, W., Jolay, L., Rodriguez, L., Fernandez, L. and Ramela, M. (1991) Autosomal recessive ectodermal dysplasia: I. An undescribed dysplasia/malformation syndrome. *Am. J. Med. Genet.*, **41**, 398–404.
46. Bancroft, J.D. and Stevens, A. (1990) *Theory and Practice of Histological Techniques.*, 3 edn. Churchill Livingstone, Edinburgh.